LANGMUIR

pubs.acs.org/Langmuir Article

Graphene Oxide Biosensors Based on Hybridization Chain Reaction Signal Amplification for Detecting Biomarkers of Radiation-Resistant Nasopharyngeal Carcinoma and Imaging in Living Cells

Lan Qin,[§] Dutao Yang,[§] Shaoxian Yin, Yue Qian, Yanfei Cai, Jian Jin, Gang Huang,* and Zhaoqi Yang*

Cite This: https://doi.org/10.1021/acs.langmuir.1c00406 Read Online

ACCESS | Metrics & More | Article Recommendations | Supporting Information

ABSTRACT: Since microRNA-205 (miRNA-205) is a predictive biomarker for antiradiation of nasopharyngeal carcinoma (NPC), quantitative detection of miRNA-205 is important for developing personalized strategies for the treatment of NPC. In this investigation, based on the graphene oxide (GO) sensor and hybridization chain reaction (HCR) for fluorescence signal amplification, a highly sensitive and selective detection method for miRNA-205 was designed. A target-recycling mechanism is employed, where a single miRNA-205 target triggers the signal amplification of many DNA signal probes. The biosensor shows the ability to analyze miRNA-205 in solution, and it can detect miRNA-205 at concentrations as low as 311.96 pM. Furthermore, the method is specific in that it distinguishes between a target miRNA and a sequence with single-, double-, and three-base mismatches, as well as other miRNAs. Considering its simplicity and superior sensitivity, it was also verified in 1‰ serum with a detection limit of 111.65 pM. Importantly, the method successfully demonstrated that miRNA-205 could be imaged in living cells, which provided the possibility of localizing target molecules in live cell imaging applications. This method has great clinical application potential in the determination of miRNA-205, a biomarker for radiation-resistant NPC.

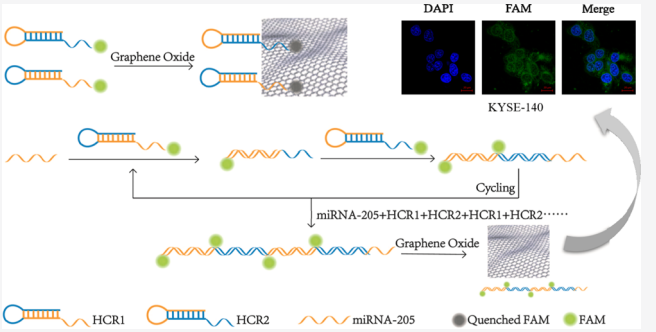

INTRODUCTION

Nasopharyngeal carcinoma (NPC) is one of the most malignant cancers, and its incidence rate ranks first among head and neck tumors. Its pathogenesis is caused by a variety of factors, and it is believed to be related to genetics, viral infections, environmental factors, and eating habits.[1] At the time of diagnosis, most patients were already in the advanced stage of nasopharyngeal cancer.[2] At present, early patients usually adopt radiation therapy, and advanced patients mainly adopt comprehensive treatment methods such as radiation therapy and chemotherapy.[3] If the patient is resistant to radiation therapy, the cure will be poor and the treatment may even be delayed. Therefore, clinical detection of radiotherapy resistance in nasopharyngeal cancer can help provide personalized strategies for the treatment, which is also a hot issue that needs to be solved in the current clinical treatment of nasopharyngeal cancer.

MircoRNA (miRNA) is a short-sequence, noncoding, single-stranded small-molecule RNA with regulatory functions and a length of about 20−24 nt.[4] A large number of studies have shown that the regulation of miRNAs plays an important role in maintaining the normal work of the organism and is closely related to the occurrence and development of many diseases in the organism, especially cancer.[5,6] There are currently more than 2000 miRNAs found in the human body, accounting for 1% of the human genome. Some scholars predict that miRNAs regulate at least one-third of human genes.[7] This suggests the importance of miRNAs in genomic regulation, and it may also be involved in regulating tumor radiotherapy resistance.[8,9] As a new biomarker, miRNA has its unique advantages in research fields such as tumor diagnosis, therapeutic targets, and prognosis evaluation. MiRNA-205 is a conserved miRNA that maintains high homology between multiple species. Existing research shows that the expression of miRNA-205 is related to nasopharyngeal, ovarian, breast, and nonsmall cell lung cancer.[10,11] MiRNA-205 is involved in radioresistance of NPC by directly targeting PTEN. Therefore, miRNA-205 is a predictive biomarker for radiosensitivity of NPC and can be used as a successful target for radiotherapy for NPC.[12,13]

MiRNAs have poor stability, are small molecules, and possess high sequence homology, which can interfere with the accuracy of detection. At present, the methods commonly used for quantitative detection of miRNA include Northern

Received: February 10, 2021
Revised: July 22, 2021

hybridization, real-time quantitative polymerase chain reaction (PCR), and microarray methods. Northern blot is the earliest established method, which has the disadvantages of being time-consuming and labor-intensive, and has low sensitivity, large sample usage, and low efficiency.[14,15] Real-time polymerase chain reaction (PCR) is prone to mix with a small amount of precursor RNA during the preparation of miRNA samples, and hence the detection results are easily interfered by precursor RNA.[16,17] The microarray method belongs to a high-throughput detection scheme, which has high detection cost, low detection sensitivity, poor detection specificity, and poor repeatability.[18,19] According to the importance of detecting the marker of radiosensitivity of NPC, two simple ways were reported in our previous work.[20,21] However, a highly sensitive method for quantitative detection of miRNA-205 needs to be developed.

Graphene oxide (GO) is a single layer of folds, and its surface contains two structures at the same time: an aromatic region and a highly oxidized region.[22] The aromatic region is mainly composed of sp^2 carbon atoms, and there are a large number of π electrons in its structure. The surface of the high oxidation zone contains a large number of oxygen-containing functional groups such as hydroxyl, carboxyl, and epoxy groups.[23] GO has a high-efficiency quenching ability, and the fluorescently labeled oligonucleotide is adsorbed on its surface by $\pi-\pi$ action, so that the fluorescence is reduced to a minimum.[24,25] When adding a nucleic acid molecule that matches the labeled oligonucleotide, the two form a stable double-stranded structure by the principle of base complementary pairing. The adsorption capacity of GO on the double-stranded structure is significantly reduced, so that the double-stranded structure can be detached from the surface of the GO, and eventually the fluorescence signal of the system is restored. Based on this principle, oligonucleotide-based GO sensor can be designed for wide application in the field of gene detection.

To detect low concentrations of disease-related genes, many amplification strategies for the detection of genes have been developed, including the ligase chain reaction (LCR),[26] rolling circle amplification (RCA),[27] and enzyme-assisted target recovery.[21] Compared with these assays, hybridization chain reaction (HCR) can accomplish the self-assembly of two hairpins with partial complementarities into long double-stranded DNA structures with sticky ends in the presence of an initiator DNA under mild conditions.[28] Therefore, HCR has been regarded as an ideal choice for nucleic acid amplification detection in complex biological samples. Herein, the GO biosensor based on the HCR is used to amplify the fluorescence signal for the high-sensitivity quantitative detection of miRNA-205, and the detection method is successfully applied to biological samples. Compared with our previous studies, HCR not only amplifies the signal but also has significant advantages such as isothermal, nonenzyme, simple operation, and low cost.

MATERIALS AND METHODS

Chemicals. Tromethamine (Tris), boric acid (H_3BO_3), disodium ethylenediamine tetraacetate (EDTA-2Na), acrylamide (C_3H_5NO), *N*,*N*′-methylenebisacrylamide ($C_7H_{10}N_2O_2$), and ammonium persulfate (APS) were purchased from China National Pharmaceutical Group Corp. DNA ladder (10−300 bp) and ethidium bromide were purchased from Thermo Fisher Scientific. These reagents are used for electrophoretic gel preparation and electrophoresis experiments. Graphene oxide (XF020, 50−200 nm) was purchased from Nanjing XFNANO Materials Tech. Co., Ltd. Tetramethylethylenediamine (TEMED) for electrophoretic gel preparation, fluorescent oligonucleotide (H1 and H2), and target RNA (all sequences used in this investigation are shown in Table S1) were purchased by Shanghai Sangon Biotechnology Co., Ltd. Sodium phosphate−sodium chloride (SPSC) buffer solution (0.75 M NaCl, 50 mM $Na_2HPO_4{\cdot}12H_2O$, pH = 7.4) was prepared using diethylpyrocarbonate (DEPC) water (water is treated with diethylpyrocarbonate and certified nuclease-free). Fluorescence spectra were obtained from a Hitachi F-7000 spectrophotometer (Hitachi Ltd., Japan). The samples placed in quartz cuvettes were excited at a wavelength of 480 nm and all emission spectra were collected at wavelengths ranging from 500 to 600 nm at room temperature. HepG2 and KYSE-150 cells were purchased from Chinese Academy of Sciences, and KYSE-140 cells were purchased from Deutsche Sammlung von Mikroorganismen und Zellkulturen. RPMI medium 1640, basic for cell culture, was purchased from Gibco Co., Ltd. Fetal bovine serum (FBS) was purchased from Zhejiang Tianhang Biotechnology Co., Ltd.

Feasibility Analysis. Seven samples were prepared with SPSC buffer to observe the fluorescence intensity and analyze the feasibility. Sample 1 is the H1 solution with a final concentration of 100 nM; sample 2 is the H2 solution with a final concentration of 100 nM; sample 3 is a mixed solution of H1 and H2, each with a final concentration of 100 nM; sample 4 is the solution obtained by mixing H1 and H2 with a final concentration of 100 nM and 120 μg/mL GO solution for 10 min; sample 5 is a solution in which 100 nM H1 and 200 nM miRNA-205 were allowed to react at 25 °C for 2 h and then 120 μg/mL of GO was added and mixed for 10 min; sample 6 is a solution in which 100 nM H2 and 200 nM miRNA-205 were allowed to react at 25 °C for 2 h and 120 μg/mL of GO was added and mixed for 10 min; sample 7 is a solution in which 100 nM H1, 100 nM H2, and 200 nM miRNA-205 were allowed to react at 25 °C for 2 h and 120 μg/mL of GO was added and mixed for 10 min. The fluorescence intensity of each sample was measured separately.

Native polyacrylamide gel electrophoresis (Native-PAGE) was used to analyze the nucleic acid chain structure after the HCR. Four samples were prepared for electrophoresis: sample 1 is the H1 solution with a final concentration of 100 nM; sample 2 is the H2 solution with a final concentration of 100 nM; sample 3 is a mixed solution of H1 and H2, each with a final concentration of 100 nM; sample 4 is a solution in which 100 nM H1, 100 nM H2, and 200 nM miRNA-205 were allowed to react at 25 °C for 2 h. In 50 mL of 15% nondenaturing acrylamide solution, 400 μL of 10% APS solution and 40 μL of TEMED solution were added, mixed quickly, poured into a glass plate, and retained for about 30 min for it to solidify. The sample was inserted into the sample well with an injector, and electrophoresis was performed at 400 V, 30 mA, and 12 W for 2 h. After the electrophoresis was completed, the gel was peeled off and immersed in 100 mL of ethidium bromide solution. After 1 h of staining, the gel was washed for gel imaging.

Optimization of Reaction Conditions. Optimization of GO concentration: H1 and H2 solutions at a final concentration of 100 nM were mixed and allowed to react at 25 °C for 2 h. Then, different volumes of the GO solution were added and made up with SPSC buffer. The final volume was 200 μL, so that the GO concentrations in the final mixed system were 0, 20, 40, 60, 80, 100, 120, 140, and 160 μg/mL. After mixing, the solution was incubated at room temperature for 10 min and its fluorescence intensity was measured.

Optimization of hairpin oligonucleotide concentration: The miRNA-205 solution at a final concentration of 200 nM was mixed with different volumes of H1 and H2 solutions, and allowed to react at 25 °C for 2 h and then 140 μg/mL of GO solution was added. The volume was made up to 200 μL with SPSC buffer so that the H1 and H2 solution concentrations in the final mixed system were 25, 50, 75, 100, 125, 150, and 175 nM. After mixing, the solution was incubated at room temperature for 10 min and its fluorescence intensity was measured.

Optimization of the reaction temperature: 100 nM of H1 and H2 was mixed with 200 nM miRNA-205 solution and allowed to react at

https://doi.org/10.1021/acs.langmuir.1c00406
Langmuir XXXX, XXX, XXX−XXX

Scheme 1. Schematic Representation of miRNA-205 Detection Based on HCR-Assisted Signal Amplification

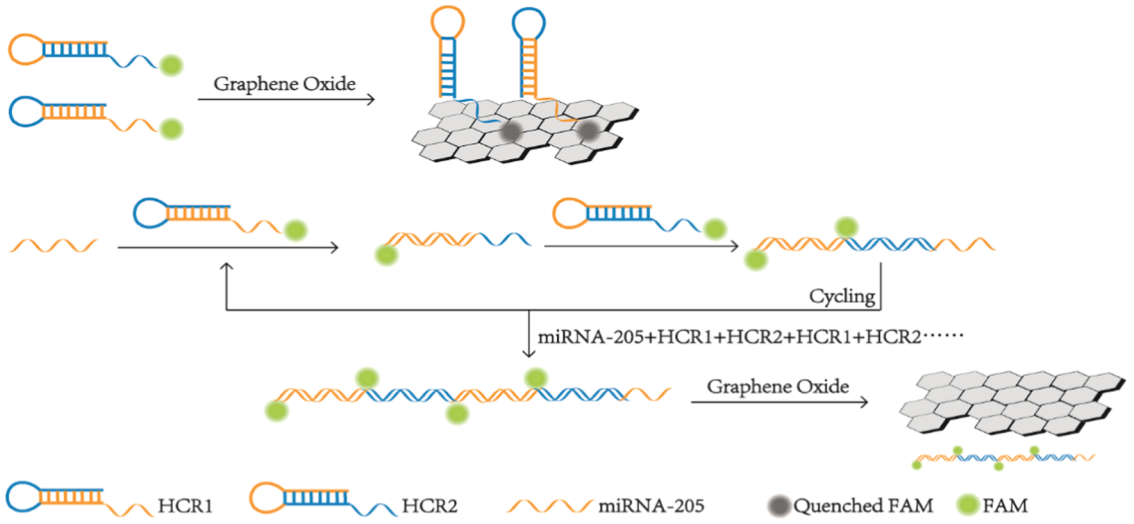

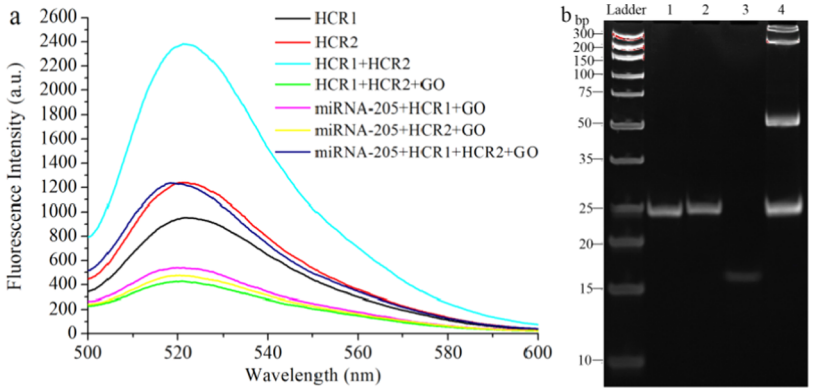

Figure 1. Feasibility analysis of the GO sensor based on the HCR. (a) Comparison of fluorescence spectra in different samples. (b) Native-PAGE analysis of HCR samples of different components. The lane 1 sample is H1, lane 2 sample is H2, lane 3 sample is miRNA-205, and lane 4 samples contain H1, H2, and miRNA-205.

25 or 37 °C for 2 h. Then, 140 μg/mL GO solution was added and made up to 200 μL with SPSC buffer. After mixing, the solution was incubated at room temperature for 10 min and its fluorescence intensity was measured.

Optimization of the reaction time: 100 nM of H1 and H2 was mixed with 200 nM miRNA-205 solution and allowed to react at 25 °C for different durations (0, 10, 20, 30, 40, 50, 60, 120, 180, 240 min). Then, 140 μg/mL GO solution was added and the volume was made up to 200 μL with SPSC buffer. After mixing, the solution was incubated at room temperature for 10 min and its fluorescence intensity was measured.

MiRNA-205 Detection. H1 and H2 (100 nM each) were mixed with miRNA-205 solution in different volumes, and allowed to react at 25 °C for 2 h. Then, 140 μg/mL GO solution was added and the volume was made up to 200 μL with SPSC buffer. The concentrations of miRNA-205 in the final mixed system were 0, 0.2, 0.3, 0.4, 0.5, 0.6, 0.7, 0.8, 0.9, 1, 10, 20, 30, 40, 50, 100, 150, and 200 nM. After mixing, the solution was incubated at room temperature for 10 min and its fluorescence intensity was measured.

Specificity Experiments. H1 and H2 (100 nM each) were mixed with 200 nM different RNA sequence (NC, miRNA-21, Let-7a, miRNA-141, RM3, RM2, RM1, miRNA-205) solutions, and allowed to react at 25 °C for 2 h. Then, 140 μg/mL GO solution was added and the volume was made up to 200 μL with SPSC buffer. After mixing, the solution was incubated at room temperature for 10 min and its fluorescence intensity was measured.

Recovery Rate in 1‰ FBS. FBS (0.2 μL) and 100 nM H1 and H2 were mixed with the miRNA-205 solution at different concentrations. After the reaction at 25 °C for 2 h, 140 μg/mL GO solution was added and the volume was made up to 200 μL with SPSC buffer. The concentrations of miRNA-205 in the final sample were 0.2, 0.4, 0.6, 0.8, and 1 nM. After mixing, the solution was incubated at room temperature for 10 min, its fluorescence intensity was measured. The measured concentration was calculated by substituting into $F = 201.53X + 337.91$, a linear equation derivesd from the concentration of miRNA-205 and corresponding fluorescence intensity in the process of miRNA-205 detection, compared with the spiked concentration, and the recovery and relative standard deviation (RSD) values were calculated.

Confocal Imaging. HepG2, KYSE-150, and KYSE-140 cells were removed and seeded each in a confocal dish. The number of seeded cells was 3×10^4, and the cells were cultured at 37 °C, 5% CO_2 incubator for 24 h. The hairpin at a concentration of 100 nm was mixed with 180 μg/mL GO for 2 h to ensure that H1 and H2 were fully adsorbed on the surface of GO. The mixed system was cocultured with three kinds of cells for 6 h. After 6 h incubation, the cells were washed with 1 mL of PBS five times. Then, the nucleus was stained with 4′,6-diamino-2-phenylindole (DAPI) solution. After staining, the cells were washed with 1 mL of PBS five times. Finally, confocal imaging was performed at an excitation wavelength of 488 nm.

RESULTS AND DISCUSSION

Detection Principle. Previous studies have shown that different sizes of graphene oxide cause different degrees of

https://doi.org/10.1021/acs.langmuir.1c00406
Langmuir XXXX, XXX, XXX−XXX

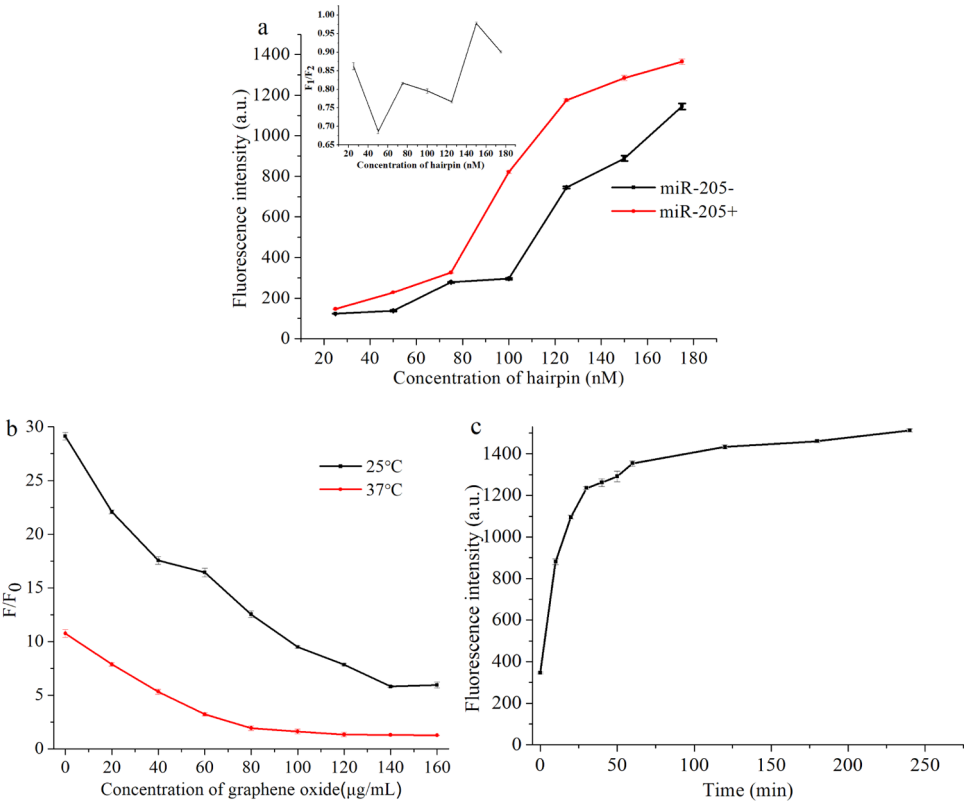

Figure 2. Optimization of reaction conditions. (a) Optimization of hairpin probe concentration. (b) Quenching of different GO concentrations at 25 and 37 °C. (c) Effects of different durations on fluorescence recovery. F is the fluorescence intensity under the respective target and F_0 corresponds to the fluorescence intensity of the system in the absence of the target (n = 3).

oxidative stress in the cells and the lateral dimensions below 200 nm seldom induce oxidative stress.[29−31] To avoid causing certain damage to cells by graphene oxide and to ensure the reliability of the sensor, graphene oxide (lateral dimensions: 50−200 nm) was purchased from the company by strict quality control and used in our study. HCR is an isothermal nucleic acid signal amplification technology. The hybridization reaction between two stable hairpin structures were started by the addition of a trigger strand miRNA-205. As shown in Scheme 1, two hairpin oligonucleotides H1 and H2 were designed, which were partially complementary and had FAM fluorescence at the sticky ends. When no trigger strand miRNA-205 is present, the sticky ends of the two hairpin oligonucleotides were adsorbed on the surface of GO, during which the fluorescence is quenched. When the trigger strand miRNA-205 was present, the secondary structure of the first hairpin H1 was opened by the trigger strand, and the exposed sticky ends open the secondary structure of the second hairpin structure H2, at which time H2 sticky ends were exposed. The sticky ends were the same as the sequence of the trigger chain, which repeatedly causes the structure of the hairpin oligonucleotides to open. Finally, a hybrid double-stranded copolymer with a sticky end was formed, which cannot be adsorbed by GO, and hence the fluorescence is not quenched. In this method, miRNA-205 was used as a trigger strand to trigger a HCR, and fluorescence recovery was initiated by opening two hairpin oligonucleotides containing FAM fluorescent group labels. The miRNA-205 can be quantitatively detected by detecting the fluorescence intensity in the system.

Feasibility Analysis. To verify the feasibility of this design, seven samples were prepared for spectral analysis. As shown in Figure 1a, the initial fluorescence intensities of H1 and H2 were slightly different. When GO was added to the H1 and H2 mixed system, the fluorescence signal was significantly reduced. This phenomenon confirms that GO can tightly adsorb H1 and H2 hairpin probes to the surface through their sticky ends, resulting in effective fluorescence quenching. When miRNA-205 was added to the H1 and GO systems, only a simple hybridization of miRNA-205 and H1 occurred and the fluorescence slightly recovered. When miRNA-205 was added to the H2 and GO systems, no reaction occurred and the fluorescence intensity hardly changed. When miRNA-205 was added to the mixture of H1 and H2, a significant fluorescence enhancement was still observed in the presence of GO, indicating that a large amount of fluorescence was recovered and miRNA-205 successfully triggered the HCR.

The feasibility of HCR was also analyzed using 15% native-PAGE. Figure 1b shows that lane 1 sample is H1, lane 2 sample is H2, and lane 3 sample is miRNA-205, where the length of H1 and H2 are 44 nt and the length of miRNA-205 is 22 nt. In lane 4 samples containing H1, H2, and miRNA-205, hybrid double-stranded copolymer bands of different lengths appeared. This proves that miRNA-205 successfully triggers the HCR as a trigger strand and forms a long double strand by continuously opening the hairpin structure. The principle of the amplification strategy based on the HCR is feasible.

Optimization of Assay Conditions. When the concentrations of H1 and H2 are both fixed at 100 nM, the quenching effect of fluorescent groups by different GO concentrations will be greatly different. As shown in Figure 2b, at increasing concentrations of GO, the fluorescence signal decreases rapidly. When the concentration exceeds 140 μg/mL, the

https://doi.org/10.1021/acs.langmuir.1c00406
Langmuir XXXX, XXX, XXX−XXX

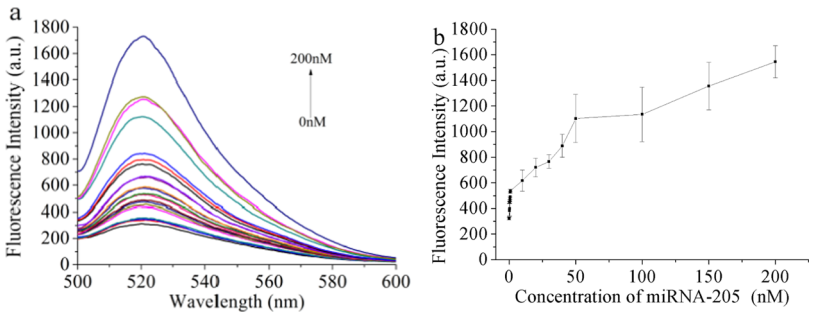

Figure 3. Detection of miRNA-205 at different concentrations based on the HCR. (a) Fluorescence spectra of miRNA-205 at different concentrations. (b) Fluorescence relationship between intensity and concentration of miRNA-205. The inset shows the linearity of fluorescence intensity relative to the concentration of miRNA-205 (n = 3).

decreased rate of fluorescence intensity will will be slight. If the concentration of GO continues to increase, the fluorescence intensity hardly changes, indicating that the concentration of GO is close to saturation. Therefore, a GO concentration of 140 μg/mL was selected during subsequent experiments to ensure that the hairpin probe was fully quenched.

To obtain the best signal-to-noise ratio and fluorescence intensity response range, the effects of the concentration of two hairpin oligonucleotides on signal intensity and fluorescence background were studied. The results are shown in Figure 2a. When the concentrations of GO and miRNA-205 are fixed, the fluorescence signal intensity (red curve) and fluorescence background intensity (black curve) of the mixed solution both increase with the increase in the concentration of the hairpin oligonucleotide. The inset in Figure 2a shows the relative fluorescence intensity, which is defined as the ratio between the fluorescence signal intensity and the fluorescence background intensity. As the concentration of hairpin oligonucleotides increased from 25 to 175 nM, the relative fluorescence intensity increased first and then decreased. When the concentration of two hairpin oligonucleotides is less than 100 nM, more hairpin probes may produce stronger signal amplification. When the concentration of the two hairpin oligonucleotides exceeds 100 nM, the relative fluorescence intensity decreases with increasing concentration, which may be because the concentration of the added hairpin probe is too high, and GO cannot completely quench the fluorescence of the FAM signal. Finally, the optimal concentration of 100 nM was determined during subsequent experiments.

HCR do not need to control temperature changes and avoid the use of enzymes, so they are simple to operate and widely used by researchers. However, the reaction temperature currently used in such literature reports is generally 25[32,33] or 37 °C.[34,35] For this reason, a comparative experiment at two temperatures on the HCR was carried out. As shown in Figure 2b, at different GO concentrations, compared with 37 °C, the initial fluorescence intensity at 25 °C is higher, and the fluorescence response range is larger, so 25 °C is selected as the reaction temperature. F is the fluorescence intensity under the respective target, and F_0 corresponds to the fluorescence intensity of the system in the absence of the target (n = 3).

The reaction time is also an important factor affecting the HCR. If the time is too short, double-strand formation will be insufficient, and if the time is too long, although double strands will continue to form, excessively long double-stranded structures will increase the system instability and reduce the reaction speed. Figure 2c shows the effect of reaction time on the recovery of fluorescence signals when miRNA-205 participates in the reaction. The fluorescence intensity recovers quickly and then gradually balances. When the reaction time exceeds 60 min, the reaction has basically reached equilibrium. To achieve the maximum fluorescence recovery effect, 60 min is selected as the best reaction time.

Sensitivity of miRNA-205 Detection Assay. The results of detecting miRNA-205 by a GO sensor based on the HCR under various optimal conditions are shown in Figure 3. As the miRNA-205 concentration (0, 0.2, 0.3, 0.4, 0.5, 0.6, 0.7, 0.8, 0.9, 1, 10, 20, 30, 40, 50, 100, 150, 200 nM) gradually increases, the fluorescence intensity also gradually increases (Figure 3a). Figure 3b is a graph drawn from the fluorescence intensity at 520 nm of the fluorescence spectrum of the biosensor according to Figure 3a, showing the change in the fluorescence intensity with the concentration of miRNA-205. When the concentration of miRNA-205 is in the range of 0−1 nM, the fluorescence intensity is linearly related to the concentration of miRNA-205. When the concentration of miRNA-205 is higher than 1 nM, the increased rate of fluorescence intensity gradually decreases, which indicates that the concentration of miRNA-205 has gradually saturated, and further addition of miRNA-205 does not significantly increase the relative fluorescence intensity. According to the fit model Logarithm (Log3P1) and formula $y = A - B*\ln(x + C)$, the limit of detection (LOD) is calculated to be 311.96 pM (detailed calculation is shown in the Supporting Information). It is shown that the combination of the HCR and GO can realize the amplification of fluorescence signal and high-sensitivity detection of miRNA-205.

Specificity of miR-205 Detection. Considering the high sequence similarity of miRNAs, experiments were performed to verify the specificity of the design. Random sequence RNA (NC), miRNA-21, Let-7a, miRNA-141, three-base mismatch targets (Rm3), two-base mismatch targets (Rm2), one-base mismatch target (Rm1), and miRNA-205 were introduced into the sensor, and the respective fluorescence spectra were recorded. The fluorescence change of each target at a wavelength of 520 nm ($F/F_0 - 1$) was compared. As shown in Figure 4, noncomplementary targets (NC, miRNA-21, Let-7a, and miRNA-141) do not cause significant fluorescence signal changes. As the number of mismatched bases decreases, the fluorescence change rate gradually increases, and RNA with one-base mismatch has only about half the change in the fluorescence signal relative to the target RNA. The oligonucleotides have weak affinity to other RNAs, so the addition of other RNAs will not affect the adsorption of GO on oligonucleotides, and the fluorescent groups carried by oligonucleotides can still be effectively quenched by GO.

https://doi.org/10.1021/acs.langmuir.1c00406
Langmuir XXXX, XXX, XXX−XXX

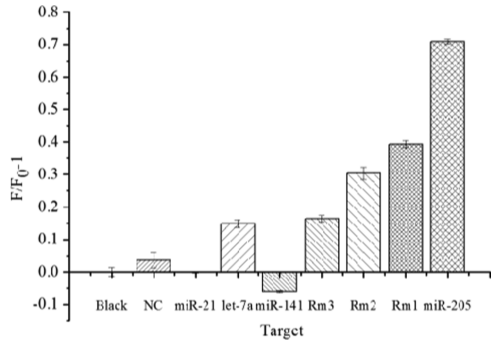

Figure 4. Specificity of different targets in HCR-based GO sensors.

Therefore, this method can distinguish the target miRNA from mismatched and noncomplementary miRNAs significantly, and has excellent specificity for miRNA-205 detection.

Optimization of Experimental Conditions in FBS. In biological samples filled with nontarget biomolecules, the adsorbed probe DNA will be nonspecific, displaced by crowded biomolecules, which is the main obstacle to the practical application of graphene oxide biosensors. Considering the difference in the composition of the buffer and FBS, the dilution factor of FBS was optimized first. As shown in Figure S1, when the dilution factor is 1‰, the difference between the original fluorescence intensity and the fluorescence intensity after quenching is larger, which is convenient for the experiment. In addition, the effect of GO concentration is discussed. Figure S2 shows that when the concentrations of H1 and H2 are both fixed at 100 nM, the fluorescence intensity does not decrease significantly when the GO concentration exceeds 180 μg/mL. Therefore, a concentration of 180 μg/mL GO was selected in subsequent experiments to ensure that the hairpin probe was completely quenched.

Feasibility Analysis in 1‰ FBS. The HCR sensor in the buffer solution realizes high-sensitivity and specificity detection of miRNA-205 and is considered for further application in biological samples. The feasibility of constructing a GO sensor based on HCR in 1‰ FBS was first performed. Eight samples were prepared. As shown in Figure S3, the results of fluorescence microscopy imaging are clearly visible. 1‰ FBS has no fluorescence (sample a). When there are only H1, H2, and GO in 1‰ FBS, the fluorescence is quenched (sample b), and the fluorescence brightness increases with the increase of miRNA-205 concentration in the reaction system (samples c−g). Sample h was the original fluorescence intensity of H1 and H2 in 1‰ FBS. It was confirmed that the detection method is suitable for the 1‰ FBS environment.

MiRNA-205 Detection in 1‰ FBS. Figure 5 shows the results of detecting miRNA-205 under optimal conditions by a sensor based on the HCR in 1‰ bovine serum. When the concentration of miRNA-205 (0, 0.2, 0.3, 0.4, 0.5, 0.6, 0.7, 0.8, 0.9, 1, 3, 5, 7, 10, 20, 30, 40, 50, 100, 150, 200 nM) increases, the fluorescence intensity also gradually increases (Figure 5a). Figure 5b is a graph plotting the fluorescence intensity at 520 nm according to the fluorescence spectrum at different miRNA-205 concentrations as illustrated in Figure 5a, showing the change in the fluorescence intensity with the concentration of miRNA-205. The illustration in Figure 5b shows the fluorescence intensity and miRNA-205 linear relationship. When the concentration of miRNA-205 is in the range of 0−1 nM, the fluorescence intensity is linearly related to the concentration of miRNA-205. When the concentration of

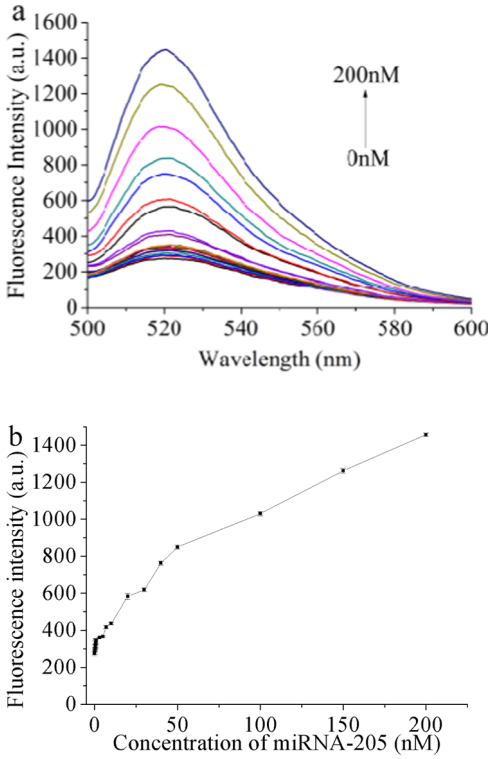

Figure 5. Detection of miRNA-205 at different concentrations in 1‰ FBS based on the HCR. (a) Fluorescence spectra of miRNA-205 at different concentrations. (b) Fluorescence relationship between intensity and concentration of miRNA-205. The inset shows the linearity of fluorescence intensity relative to the concentration of miRNA-205 (n = 3).

miRNA-205 is higher than 1 nM, the increased rate of fluorescence intensity gradually slows down, which indicates that the concentration of miRNA-205 has gradually saturated, and further increase of miRNA-205 will not significantly increase the relative fluorescence intensity. According to the fit model Logarithm (Log3P1) and formula $y = A - B*\ln(x + C)$, the LOD is calculated to be 111.65 pM (detailed calculation is shown in the Supporting Information).

Specificity Experiments in 1‰ FBS. Considering the complex environment in the serum samples, the specificity of the design was also verified. By introducing random sequence RNA (NC), miRNA-21, Let-7a, miRNA-141, three-base mismatch targets (Rm3), two-base mismatch targets (Rm2), and one-base mismatch target (Rm1), the target miRNA-205 was used to investigate the fluorescence response of the GO sensor based on the double-strand specific nuclease, recording the respective fluorescence spectrum, and comparing the fluorescence change of each target at a wavelength of 520 nm ($F/F_0 - 1$). As shown in Figure 6, noncomplementary targets (NC, miRNA-21, Let-7a, and miRNA-141) do not cause significant fluorescence signal changes. As the number of mismatched bases decreases, the fluorescence change rate gradually increases. The one-base mismatch RNA changes less than half the fluorescence signal of the target RNA. The oligonucleotide has weak affinity to other RNAs, and so the addition of other RNAs will not affect the adsorption of GO on oligonucleotides, and the fluorescent groups carried by oligonucleotides can still be effectively quenched by GO. Therefore, the design can distinguish the target miRNA from mismatched and noncomplementary miRNAs significantly.

https://doi.org/10.1021/acs.langmuir.1c00406
Langmuir XXXX, XXX, XXX−XXX

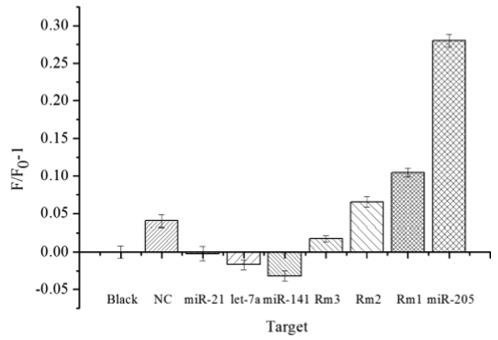

Figure 6. Specificity of HCR-based GO sensors in 1‰ FBS for different targets.

The detection method also has excellent specificity for the detection of miRNA-205 in 1‰ FBS.

Recovery Rate in 1‰ FBS. To further verify the response of the biosensor in 1‰ FBS, a recovery experiment was performed. Five known concentrations of miRNA-205 in the linear detection range of the biosensor were selected and added to 1‰ FBS. Table 1 shows that the recovery rate in 1‰ FBS is favorable, ranging from 96.74 to 122.17%, while the RSD value is always lower than 2%. This indicates that the GO biosensor based on the HCR can be successfully applied to 1‰ FBS spiked samples.

Table 1. Recovery and Detection of 1‰ FBS by Adding Standards

spiked miRNA-205 (nM)	found miRNA-205 (nM)	recovery (%)	RSD (n = 3, %)
0.2	0.16	99.42	0.44
0.4	0.45	122.17	1.69
0.6	0.62	109.02	0.25
0.8	0.76	99.21	1.24
1	0.93	96.74	1.53

Confocal Imaging in Cells. With the purpose to explore the ability of the method for imaging miRNA-205 in living cells, three cell lines with different miRNA-205 expression levels were selected for verification by confocal imaging using sensors. According to reports, the expression level of miRNA-205 is different in different cells. The expression level is very low in HepG2 cell line and higher in KYSE-150, while KYSE-140 cell line is about twice as high as KYSE-150.[36]

The three cells were cultured stably in a confocal Petri dish, and then a GO sensor system based on the HCR was added and the culture was continued for laser confocal imaging. The imaging results are shown in Figure 7a, where almost no fluorescent spots appeared in HepG2 with low expression of miRNA-205. As anticipated, the bright fluorescent spots were found in KYSE-140 cells, which indicated that the HCR was triggered by target miRNA. The statistics of the fluorescence intensity of the spots in each cell line was exhibited in Figure 7b, the result being consistent with the visible results in Figure 7a. These findings obviously verified that the proposed method processes the ability for imaging and locating miRNA in living cells.

Quantitative Real-Time Polymerase Chain Reaction (qRT-PCR) Analysis of miR-205. A qRT-PCR experiment was carried out to detect the expression of miR-205. First, HepG2, KYSE-150, and KYSE-140 cells were cultured until the density reached 80%. The TRIzol reagent was lysed with the three kinds of cells, and the total RNA was extracted and collected. Then, using total RNA as a template, the first strand of miRNA cDNA was synthesized by RT-PCR. The expression of miR-205 was detected by qPCR with miR-205 forward primers and universal reverse primers (Figure S7).

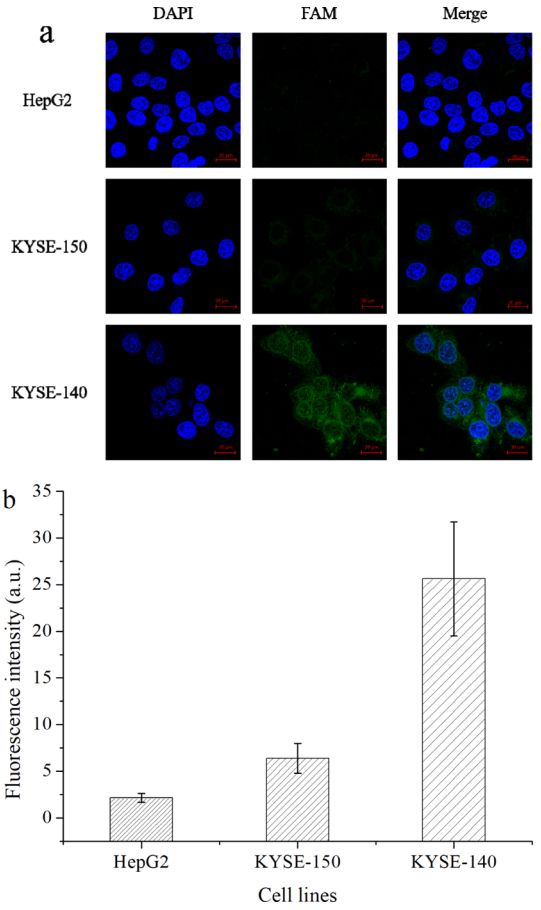

Figure 7. Confocal images of HepG2, KYSE-150, and KYSE-140 cells were cultured with HCR-based GO sensors. (a) Photographs of cells in each channel under a confocal microscope. (b) Statistics of FAM fluorescence intensity of each cell line.

CONCLUSIONS

In summary, a novel fluorescence-sensing biosensor based on the HCR and GO for the detection of miRNA-205 (biomarker for antiradiation of NPC) with excellent selectivity and high sensitivity was demonstrated in this investigation. In addition, miRNA-205 was still quantitatively detected and showed high specificity even in single mismatch discrimination when the proposed sensing platform was applied to the complicated environment of serum. The linear detection range of the presented strategy is 0−1 nM, the correlation coefficient is R^2 = 0.994, and the LOD is 111.65 pM (in 1‰ serum). More importantly, we have successfully verified the application of our designed platform for ultrasensitive detection of miRNA-205 in cell samples. The results also revealed that the presented strategy could indicate the localization of target miRNA in living cells by displaying intense fluorescence spots. It is also our hope that the outcomes from this study could provide a promising platform for the biomarker detection in clinical diagnostics as well as applied in imaging for cell biology.

https://doi.org/10.1021/acs.langmuir.1c00406
Langmuir XXXX, XXX, XXX−XXX

■ ASSOCIATED CONTENT

Supporting Information

The Supporting Information is available free of charge at https://pubs.acs.org/doi/10.1021/acs.langmuir.1c00406.

Nucleic acid sequences used in the investigation, optimization of FBS dilution ratio, optimization of GO concentration, feasibility analysis of HCR sensor, characterization of GO, relative cell viability at different concentrations of GO, feasibility analysis of graphene oxide sensor, qRT-PCR analysis of miR-205 in three cells, and relationship between fluorescence intensity and concentration of miR-205 (PDF)

■ AUTHOR INFORMATION

Corresponding Authors

Gang Huang − *Shanghai Key Laboratory of Molecular Imaging, Shanghai University of Medicine and Health Sciences, Shanghai 201318, P. R. China*; Email: huanggang@sumhs.edu.cn

Zhaoqi Yang − *School of Pharmaceutical Sciences, Jiangnan University, Wuxi 214122, P. R. China*; orcid.org/0000-0002-4485-8872; Phone: +86 510 85918219; Email: zhaoqiyang@jiangnan.edu.cn

Authors

Lan Qin − *School of Pharmaceutical Sciences, Jiangnan University, Wuxi 214122, P. R. China*

Dutao Yang − *School of Pharmaceutical Sciences, Jiangnan University, Wuxi 214122, P. R. China*

Shaoxian Yin − *School of Pharmaceutical Sciences, Jiangnan University, Wuxi 214122, P. R. China*

Yue Qian − *School of Pharmaceutical Sciences, Jiangnan University, Wuxi 214122, P. R. China*

Yanfei Cai − *School of Pharmaceutical Sciences, Jiangnan University, Wuxi 214122, P. R. China*

Jian Jin − *School of Pharmaceutical Sciences, Jiangnan University, Wuxi 214122, P. R. China*

Complete contact information is available at: https://pubs.acs.org/10.1021/acs.langmuir.1c00406

Author Contributions

§L.Q. and D.Y. contributed equally to this work.

Notes

The authors declare no competing financial interest.

■ ACKNOWLEDGMENTS

The authors greatly appreciate the Top-notch Academic Programs Project of Jiangsu Higher Education Institutions (PPZY2015B146), the Wuxi Science and Technology Development Fund (N20192044), the 2018 Innovative Research Team of Jiangsu Province, National Natural Science Foundation of China (No. 81830052), the Construction Project of Shanghai Key Laboratory of Molecular Imaging (18DZ2260400), and the Shanghai Municipal Education Commission (Class II Plateau Disciplinary Construction Program of Medical Technology of SUMHS, 2018−2020) for supporting this research work.

■ REFERENCES

(1) Xie, X.; Lin, W.; Zheng, W.; Chen, T.; Yang, H.; Sun, L.; Huang, F.; Wang, Z.; Lin, H.; Chen, L.; Liu, J.; Yang, L. Downregulation of G2/mitotic-specific cyclinB1 triggers autophagy via AMPK-ULK1-dependent signal pathway in nasopharyngeal carcinoma cells. *Cell Death Dis.* **2019**, *10*, No. 94.

(2) Ding, H.; Cai, Y.; Gao, L.; Liang, M.; Miao, B.; Wu, H.; Liu, Y.; Xie, N.; Tang, A.; Fan, K.; Yan, X.; Nie, G. Exosome-like Nanozyme Vesicles for H_2O_2-Responsive Catalytic Photoacoustic Imaging of Xenograft Nasopharyngeal Carcinoma. *Nano Lett.* **2019**, *19*, 203−209.

(3) Shu, C.; Zheng, W.; Lin, K.; Lim, C.; Huang, Z. Label-Free Follow-Up Surveying of Post-Treatment Efficacy and Recurrence in Nasopharyngeal Carcinoma Patients with Fiberoptic Raman Endoscopy. *Anal. Chem.* **2021**, *93*, 2053−2061.

(4) Lu, T. X.; Rothenberg, M. E. MicroRNA. *J. Allergy Clin. Immunol.* **2018**, *141*, 1202−1207.

(5) Ambros, V. The functions of animal microRNAs. *Nature* **2004**, *431*, 350−355.

(6) Mishra, S.; Yadav, T.; Rani, V. Exploring miRNA based approaches in cancer diagnostics and therapeutics. *Crit. Rev. Oncol. Hematol.* **2016**, *98*, 12−23.

(7) Chang, T. C.; Mendell, J. T. microRNAs in vertebrate physiology and human disease. *Annu. Rev. Genomics Hum. Genet.* **2007**, *8*, 215−239.

(8) Li, A. L.; Chung, T. S.; Chan, Y. N.; Chen, C. L.; Lin, S. C.; Chiang, Y. R.; Lin, C. H.; Chen, C. C.; Ma, N. microRNA expression pattern as an ancillary prognostic signature for radiotherapy. *J. Transl. Med.* **2018**, *16*, No. 341.

(9) Li, H.; Jin, X.; Chen, B.; Li, P.; Li, Q. Autophagy-regulating microRNAs: potential targets for improving radiotherapy. *J. Cancer Res. Clin. Oncol.* **2018**, *144*, 1623−1634.

(10) Duan, B.; Guo, T.; Sun, H.; Cai, R.; Rui, Q.; Xi, Z. miR-205 as a biological marker in non-small cell lung cancer. *Biomed. Pharmacother.* **2017**, *91*, 823−830.

(11) He, L.; Zhu, W.; Chen, Q.; Yuan, Y.; Wang, Y.; Wang, J.; Wu, X. Ovarian cancer cell-secreted exosomal miR-205 promotes metastasis by inducing angiogenesis. *Theranostics* **2019**, *9*, 8206−8220.

(12) Wang, D.; Wang, S.; Liu, Q.; Wang, M.; Wang, C.; Yang, H. SZ-685C exhibits potent anticancer activity in both radiosensitive and radioresistant NPC cells through the miR-205-PTEN-Akt pathway. *Oncol. Rep.* **2013**, *29*, 2341−2347.

(13) Qu, C.; Liang, Z.; Huang, J.; Zhao, R.; Su, C.; Wang, S.; Wang, X.; Zhang, R.; Lee, M. H.; Yang, H. MiR-205 determines the radioresistance of human nasopharyngeal carcinoma by directly targeting PTEN. *Cell Cycle* **2012**, *11*, 785−796.

(14) De la Rosa, C.; Reyes, J. L. Northern Blot Analysis of microRNAs and Other Small RNAs in Plants. *Methods Mol. Biol.* **2019**, *1932*, 121−129.

(15) Pall, G. S.; Hamilton, A. J. Improved northern blot method for enhanced detection of small RNA. *Nat. Protoc.* **2008**, *3*, 1077−1084.

(16) Chen, C.; Ridzon, D. A.; Broomer, A. J.; Zhou, Z.; Lee, D. H.; Nguyen, J. T.; Barbisin, M.; Xu, N. L.; Mahuvakar, V. R.; Andersen, M. R.; Lao, K. Q.; Livak, K. J.; Guegler, K. J. Real-time quantification of microRNAs by stem-loop RT-PCR. *Nucleic Acids Res.* **2005**, *33*, No. e179.

(17) Thorsen, M.; Blondal, T.; Mouritzen, P. Quantitative RT-PCR for MicroRNAs in Biofluids. *Methods Mol. Biol.* **2017**, *1641*, 379−398.

(18) Dell'Aversana, C.; Giorgio, C.; Altucci, L. MicroRNA Expression Profiling Using Agilent One-Color Microarray. *Methods Mol. Biol.* **2017**, *1509*, 169−183.

(19) Mastriani, E.; Zhai, R.; Zhu, S. Microarray-Based MicroRNA Expression Data Analysis with Bioconductor. *Methods Mol. Biol.* **2018**, *1751*, 127−138.

(20) Yang, Z.; Qin, L.; Yang, D.; Hu, Q.; Jin, J. A graphene oxide fluorescent sensing platform for sensitive and specific detecting biomarker of radiation-resistant nasopharyngeal carcinoma. *Bioorg. Med. Chem. Lett.* **2019**, *29*, 2383−2386.

(21) Yang, Z.; Qin, L.; Yang, D.; Chen, W.; Qian, Y.; Jin, J. Signal amplification method for miR-205 assay through combining graphene oxide with duplex-specific nuclease. *RSC Adv.* **2019**, *9*, 27341−27346.

(22) Liu, Y.; Yu, D.; Zeng, C.; Miao, Z.; Dai, L. Biocompatible graphene oxide-based glucose biosensors. *Langmuir* **2010**, *26*, 6158−6160.
(23) Wang, Y.; Li, Z.; Wang, J.; Li, J.; Lin, Y. Graphene and graphene oxide: biofunctionalization and applications in biotechnology. *Trends Biotechnol.* **2011**, *29*, 205−212.
(24) Lu, C.; Huang, P. J.; Liu, B.; Ying, Y.; Liu, J. Comparison of Graphene Oxide and Reduced Graphene Oxide for DNA Adsorption and Sensing. *Langmuir* **2016**, *32*, 10776−10783.
(25) Morales-Narvaez, E.; Merkoci, A. Graphene Oxide as an Optical Biosensing Platform: A Progress Report. *Adv. Mater.* **2019**, *31*, No. e1805043.
(26) Yan, J.; Li, Z.; Liu, C.; Cheng, Y. Simple and sensitive detection of microRNAs with ligase chain reaction. *Chem. Commun.* **2010**, *46*, 2432−2434.
(27) Orbach, R.; Guo, W.; Wang, F.; Lioubashevski, O.; Willner, I. Self-assembly of luminescent Ag nanocluster-functionalized nanowires. *Langmuir* **2013**, *29*, 13066−13071.
(28) Huang, J.; Gao, X.; Jia, J.; Kim, J. K.; Li, Z. Graphene oxide-based amplified fluorescent biosensor for Hg(2+) detection through hybridization chain reactions. *Anal. Chem.* **2014**, *86*, 3209−3215.
(29) Vranic, S.; Rodrigues, A. F.; Buggio, M.; Newman, L.; White, M. R. H.; Spiller, D. G.; Bussy, C.; Kostarelos, K. Live Imaging of Label-Free Graphene Oxide Reveals Critical Factors Causing Oxidative-Stress-Mediated Cellular Responses. *ACS Nano* **2018**, *12*, 1373−1389.
(30) Fadeel, B.; Bussy, C.; Merino, S.; Vazquez, E.; Flahaut, E.; Mouchet, F.; Evariste, L.; Gauthier, L.; Koivisto, A. J.; Vogel, U.; Martin, C.; Delogu, L. G.; Buerki-Thurnherr, T.; Wick, P.; Beloin-Saint-Pierre, D.; Hischier, R.; Pelin, M.; Candotto Carniel, F.; Tretiach, M.; Cesca, F.; Benfenati, F.; Scaini, D.; Ballerini, L.; Kostarelos, K.; Prato, M.; Bianco, A. Safety Assessment of Graphene-Based Materials: Focus on Human Health and the Environment. *ACS Nano* **2018**, *12*, 10582−10620.
(31) Palmieri, V.; Perini, G.; De Spirito, M.; Papi, M. Graphene oxide touches blood: in vivo interactions of bio-coronated 2D materials. *Nanoscale Horiz.* **2019**, *4*, 273−290.
(32) Zhang, S.; Wang, K.; Li, K. B.; Shi, W.; Jia, W. P.; Chen, X.; Sun, T.; Han, D. M. A DNA-stabilized silver nanoclusters/graphene oxide-based platform for the sensitive detection of DNA through hybridization chain reaction. *Biosens. Bioelectron.* **2017**, *91*, 374−379.
(33) Fan, J.; Yuan, L.; Liu, Q.; Tong, C.; Wang, W.; Xiao, F.; Liu, B.; Liu, X. An ultrasensitive and simple assay for the Hepatitis C virus using a reduced graphene oxide-assisted hybridization chain reaction. *Analyst* **2019**, *144*, 3972−3979.
(34) Xiong, M.; Rong, Q.; Kong, G.; Yang, C.; Zhao, Y.; Qu, F. L.; Zhang, X. B.; Tan, W. Hybridization chain reaction-based nanoprobe for cancer cell recognition and amplified photodynamic therapy. *Chem. Commun.* **2019**, *55*, 3065−3068.
(35) Wang, X.; Jiang, A.; Hou, T.; Li, H.; Li, F. Enzyme-free and label-free fluorescence aptasensing strategy for highly sensitive detection of protein based on target-triggered hybridization chain reaction amplification. *Biosens. Bioelectron.* **2015**, *70*, 324−329.
(36) Kimura, S.; Naganuma, S.; Susuki, D.; Hirono, Y.; Yamaguchi, A.; Fujieda, S.; Sano, K.; Itoh, H. Expression of microRNAs in squamous cell carcinoma of human head and neck and the esophagus: miR-205 and miR-21 are specific markers for HNSCC and ESCC. *Oncol. Rep.* **2010**, *23*, 1625−1633.

https://doi.org/10.1021/acs.langmuir.1c00406
Langmuir XXXX, XXX, XXX−XXX